SAND2017-4803J

Multi-material continuum topology optimization with arbitrary volume and mass constraints

Miguel A. Aguiló, Emily Daniels, and Glaucio H. Paulino

December 18, 2016

Abstract

Presented is a framework for multi-material compliance minimization in the context of continuum based topology optimization. We adopt the common approach of finding an optimal shape by solving a series of explicit convex (linear) approximations to the volume constrained compliance minimization problem. It has been shown previously that the dual objective associated with the linearized subproblems is a separable function of the Lagrange multipliers and thus, the update of each design variable is dependent only on the Lagrange multiplier of its associated volume constraint. As a result, the simple and efficient Optimality Criteria design variable update scheme, applied in series or in parallel for each volume constraint, can be leveraged to obtain a unique solution. This formulation leads to a setting in which sufficiently general volume/mass constraints can be specified, i.e., each volume/mass constraint can control all or a subset of the candidate materials and can control the entire domain or a sub-region of the domain. Two material interpolation schemes are investigated and coupled with the presented approach. The key ideas presented herein are demonstrated through a 2D MATLAB implementation.

Keywords: topology optimization; multi-material; volume constraints; mass constraints; additive manufacturing

1 Introduction

With the rapid advancement of additive manufacturing technologies in recent years, it has become increasingly feasible to realize arbitrary geometries, e.g., designs derived from topology optimization (see e.g., Zegard and Paulino (2016)). Until recently, most additive manufacturing technologies have been limited to fabricating designs from a single material, leading to parts with little functional capability. Multi-material 3D printing is only a budding technology, but will certainly lead to increasingly functional designs. Gaynor et al. (2014) have already realized compliant mechanism designs based on three-phase (2 solid phases plus void) topology optimization using the PolyJet additive manufacturing technology, which can print bulk materials covering a wide range of elastic moduli (Stratasys, 2016). Even using single material printers, functional designs have been fabricated by varying the microstructure throughout the print to achieve varying elastic properties (Schumacher et al., 2015). The simple and efficient multi-material topology optimization algorithm presented here can accommodate an arbitrary number of candidate materials, including both fully dense or cellular materials with isotropic or anisotropic behavior. Thus, designs with varying densities and material properties can be designed and manufactured using additive manufacturing technologies that can deposit single or multiple bulk materials.

Perhaps due to the excitement surrounding additive manufacturing, the number of publications related to multi-material topology optimization in the continuum setting is growing. The great majority of work in density-based topology optimization considering multiple material phases uses some extension of the Solid Isotropic Material with Penalization (SIMP) interpolation scheme, which uses a power law to penalize intermediate densities and achieve designs with distinct solid and void regions (Bendsøe, 1989; Zhou and Rozvany, 1991). For two-material (no void) topology optimization of materials with extreme thermal expansion, Sigmund and Torquato (1997) proposed an extension of SIMP that uses a single design variable to interpolate between the two material phases. The approach has also been used to design, e.g., multi-physics actuators (Sigmund, 2001) and piezocomposites (Vatanabe et al., 2012, 2013, 2014). Sigmund and Torquato (1997)

also proposed a three-phase extension of SIMP characterized by a topology design variable that controls the material/void distribution and a second design variable that interpolates between two solid material phases. Although this "three-phase mixing scheme" has been extended further to incorporate up to m candidate materials (Stegmann and Lund, 2005), some authors claim that designs tend to get stuck in local minima when the number of materials exceeds three solid phases (Stegmann and Lund, 2005; Taheri and Suresh, 2016). Actually, most results in the literature for multi-material topology optimization using this "m-phase mixing scheme" have been limited to two solid phases plus void (Gao and Zhang, 2011; Gaynor et al., 2014; Gibiansky and Sigmund, 2000) or three-solid phases plus void (Taheri and Suresh, 2016).

Other material interpolation schemes that are better equipped to handle greater than three solid phases have also been proposed. For example, in the context of composite design via fiber orientation optimization, the Discrete Material Optimization (DMO) technique was proposed to consider an arbitrary number of materials, each characterized by a discrete fiber orientation (Stegmann and Lund, 2005; Lund and Stegmann, 2005). The DMO interpolation schemes are typically also an extension of SIMP, but differ from the m-phase mixing scheme discussed above in that each design variable represents the density of a single material. Gao and Zhang (2011) compare the DMO interpolation schemes to the m-phase mixing approach and find that DMO is able to reach superior designs, even in cases considering two solid phases plus void and a single mass constraint. However, the DMO interpolation methods do not inherently prevent the sum of material densities at a point from exceeding one as the m-phase mixing scheme does. To enforce this property when using DMO, Hvejsel and Lund (2011) and Hvejsel et al. (2011) impose a large system of sparse linear constraints and Hvejsel et al. (2011) further enforces a quadratic constraint to penalize material mixing.

Tavakoli and Mohseni (2014) use a DMO interpolation scheme coupled with an alternating active-phase algorithm, in which designs containing up to m material phases (without material mixing) are achieved by performing m binary material phase updates in an inner loop of each outer optimization iteration. Implementing this approach essentially amounts to adding a loop over an existing two-phase topology optimization code. Although this approach is flexible enough to accommodate an arbitrary number of candidate materials, the results are order-dependent, which may prevent the method from being applicable to problems considering materials with more general constitutive behavior (e.g., anisotropic or nonlinear materials). Additionally, the alternating active-phase algorithm leads to an increase in the number of finite element solves by a factor of the number of candidate materials times the number of specified inner iterations and may not scale well to large problems. Park and Sutradhar (2015) couple this alternating active-phase approach with multiresolution topology optimization (Filipov et al., 2016; Nguyen et al., 2010, 2012) to solve multi-material problems in three dimensions.

A pitfall of the DMO approaches are that the number of design variables scales linearly with the number of candidate materials. Yin and Ananthasuresh (2001) proposed a peak function material interpolation method in which the number of design variables remains constant as the number of candidate materials increases. In their approach, each material has a mean and standard deviation and using a normal distribution function a distinct material is selected when the density design variable is equal to the mean of that material. A color level-set approach was also proposed by Wang and Wang (2004) in which only m level-set functions are needed to obtain designs with 2^m materials. The method has been applied for compliant mechanism design (Wang et al., 2005) and in problems considering stress constraints (Guo et al., 2014). Multi-material designs have also been achieved using phase-field methods by e.g., Wang and Zhou (2004), Zhou and Wang (2007), Tavakoli and Mohseni (2014), and Wallin et al. (2015) and using evolutionary methods by e.g., Huang and Xie (2009).

In this work the DMO material interpolation schemes are coupled with an Optimality Criteria (OC) design variable update to achieve designs considering an arbitrary number of candidate materials and an arbitrary number of volume/mass constraints. Although the number of design variables scales linearly with the number of candidate materials and pointwise densities may exceed one, the DMO interpolations lead to linear and variable separable volume/mass constraints. Thus, a recent observation by Zhang et al. (in prep) can be exploited: multiple linear volume constraints lead to a separable Lagrangian function, allowing the design to be updated for each volume/mass constraint independently (i.e., order-independent updates) using the Optimality Criteria method. The observation facilitates sufficient flexibility in the problem statement in that volume/mass constraints can be specified to control all or a subset of the candidate materials in all or a subset of the design domain. Zhang et al. (in prep) apply the idea to the design of truss structures with possibly nonlinear materials, while here it is found to work well in the continuum setting considering linear

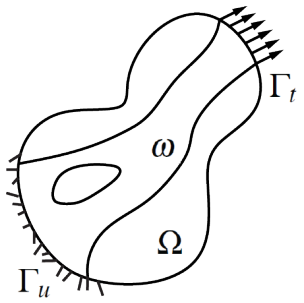

Figure 1: Topology optimization problem schematic (adapted from Talischi et al. (2012))

elastic materials. The approach is straightforward to implement and the number of finite element solves remains constant as the number of constraints increases.

The remainder of this manuscript is organized as follows: In Section 2 the problem setting and formulation for compliance minimization with generalized volume/mass constraints are provided. In addition, two DMO material interpolation schemes are presented and the sensitivities are derived. A post-processing step required for achieving physical designs is introduced in Section 3. Section 4 includes some details related to implementation of the multi-material framework in Sandia National Laboratories' platform for topology optimization, PLATO. Two numerical examples demonstrate the capabilities and potential shortcomings of the proposed approach in Section 5. Finally, in Section 6, conclusions are provided.

2 Formulation

2.1 Problem setting

Multi-material topology optimization for problems in linear elastostatics aims to find the set of material points $\omega = \{\mathbf{X} \in \mathbb{R}^{n_{sd}}\} \subset \Omega$ and the material distribution $\mathbf{C}(\mathbf{X})$ such that an objective $J(\omega, \mathbf{u})$ is extremized, an arbitrary number of constraints $g_j(\omega, \mathbf{u}) \leq 0$ are satisfied, and for which the displacement field $\mathbf{u} \in U$ satisfies the governing elastostatics equation, written in weak form here:

$$\int_{\omega} \mathbf{C}(\mathbf{X}) \nabla \mathbf{u} : \nabla \delta \mathbf{u} \, d\mathbf{X} = \int_{\Gamma_t} \mathbf{t} \cdot \delta \mathbf{u} \, ds, \qquad \forall \delta \mathbf{u} \in U_o \tag{1}$$

where Ω is a set of material points $\mathbf{X}$ in spatial dimension n_{sd} with boundary $\delta\Omega$, $\omega \subset \Omega$ defines the optimal shape, $\mathbf{C}(\mathbf{X})$ is the spatially varying material tensor, $U = \{\mathbf{u} \in H^1 : \mathbf{u} = \overline{\mathbf{u}} \text{ on } \Gamma_u\}$ is the set of kinematically admissible displacements (trial functions), $U_o = \{\delta\mathbf{u} \in H^1 : \mathbf{u} = 0 \text{ on } \Gamma_u\}$ is the set of test functions, $\Gamma_u \subset \delta\Omega$ is the portion of the boundary where displacements $\mathbf{u} = \overline{\mathbf{u}}$ are prescribed, and $\Gamma_t \subset \delta\Omega$ is the portion of the boundary where tractions $\mathbf{t} = \overline{\mathbf{t}}$ are prescribed. The scenario described above is shown in Fig. 1, which is adapted from Talischi et al. (2012).

The optimal set of material points ω can be defined by indicator function χ such that:

$$\chi(\mathbf{X}) = \begin{cases} 1 & \text{if } \mathbf{X} \in \omega \\ 0 & \text{if } \mathbf{X} \in \Omega \setminus \omega \end{cases} \tag{2}$$

and the material distribution $\mathbf{C}(\mathbf{X})$ can be defined by selecting from a finite set of $m_{\mathbf{X}}$ material tensors at each material point such that:

$$\mathbf{C}(\mathbf{X}) = \mathcal{A}(S(\mathbf{X})) \tag{3}$$

where $S(\mathbf{X}) = \{\mathbf{C}_1, \ldots, \mathbf{C}_{m_{\mathbf{X}}}\}$ is the set of material tensors for the $m_{\mathbf{X}}$ candidate materials at point $\mathbf{X}$ and $\mathcal{A}$ is a choice function for which $\mathcal{A}(S(\mathbf{X})) \in S(\mathbf{X})$ holds. With these definitions, the weak form of the governing elastostatics equation can be re-written over the entire domain Ω as:

$$\int_{\Omega} \chi\left(\mathbf{X}\right) \mathcal{A}\left(S\left(\mathbf{X}\right)\right) \nabla \mathbf{u} : \nabla \delta \mathbf{u} \, d\mathbf{X} = \int_{\Gamma_t} \mathbf{t} \cdot \delta \mathbf{u} \, ds, \qquad \forall \delta \mathbf{u} \in U_o \tag{4}$$

As posed, finding ω and $\mathbf{C}\left(\mathbf{X}\right)$ becomes a large integer programming problem, which can be impractical to solve. Thus, the indicator function χ and choice function $\mathcal{A}$ are re-cast as m continuous scalar fields $\rho_i\left(\mathbf{X}\right) \in [0,1], i = 1, \ldots, m$, each representing the density distribution of each of the m candidate materials in Ω. The total density at $\mathbf{X}$ is then $\rho_T\left(\mathbf{X}\right) = \sum_{i=1}^{m} \rho_i\left(\mathbf{X}\right) \in [0,1]$. The magnitude of these density fields can be used to determine the contribution of the m candidate materials at point $\mathbf{X}$ according to an interpolation function $\eta\left(\rho_1\left(\mathbf{X}\right), \ldots, \rho_m\left(\mathbf{X}\right), S\left(\mathbf{X}\right)\right)$. The interpolation function may also serve to penalize intermediate densities so that $\rho_i\left(\mathbf{X}\right)$ better approximates the integer problem (Bendsøe, 1989; Stolpe and Svanberg, 2001; Zhou and Rozvany, 1991) and to penalize material mixing.

It is noted that the material distribution problem with volume/mass constraints described here is known to be ill-posed in that a non-convergent sequence of solutions consisting of designs with increasingly fine perforations arises. In order to ensure existence of solutions, the density fields are filtered by convolution of a smoothing filter F and the density field (Bourdin, 2001; Bruns and Tortorelli, 2001):

$$\hat{\rho}_i\left(\mathbf{X}\right) = \left(F * \rho_i\right)\left(\mathbf{X}\right) = \int_{B_R} F\left(\mathbf{X}, \mathbf{Y}\right) \rho_i\left(\mathbf{Y}\right) d\mathbf{Y} \tag{5}$$

where $\hat{\rho}_i\left(\mathbf{X}\right)$ is the filtered density field of material i and B_R is the ball of radius R, which characterizes the filter. The material interpolation function can be re-written in terms of the filtered density fields and the governing elastostatics equation becomes:

$$\int_{\Omega} \eta\left(\hat{\rho}_1\left(\mathbf{X}\right), \ldots, \hat{\rho}_m\left(\mathbf{X}\right), S\left(\mathbf{X}\right)\right) \nabla \mathbf{u} : \nabla \delta \mathbf{u} \, d\mathbf{X} = \int_{\Gamma_t} \mathbf{t} \cdot \delta \mathbf{u} \, ds, \qquad \forall \delta \mathbf{u} \in U_o \tag{6}$$

2.2 Discretization of the elastostatics problem

The solution to (6) can be approximated via the finite element method. The domain is discretized into finite elements with degrees of freedom defined at the nodal points. The trial and test functions are approximated using interpolation (shape) functions $N_i\left(\mathbf{X}\right)$ such that $\mathbf{u}\left(\mathbf{X}\right) = \sum_{i=1}^{n_{dof}} N_i\left(\mathbf{X}\right) u_i$, where n_{dof} is the number of degrees of freedom in the finite element mesh. With this approximation of the displacement field, the governing equation written in discrete form becomes $\mathbf{K}\mathbf{u} = \mathbf{f}$, where the i, j term of the stiffness matrix $\mathbf{K}$ is:

$$K_{ij} = \int_{\Omega} \eta\left(\hat{\rho}_1\left(\mathbf{X}\right), \ldots, \hat{\rho}_1\left(\mathbf{X}\right), S\left(\mathbf{X}\right)\right) \nabla N_i : \nabla N_j \, d\mathbf{X} \tag{7}$$

and the external force applied at degree of freedom i is $f_i = \int_{\Gamma_t} \mathbf{t} \cdot N_i \, ds$.

2.3 Discretization of the optimization space

For convenience, the control points of the density fields $\rho_i\left(\mathbf{X}\right), i = 1, \ldots, m$, are defined in accordance with the finite element discretization, either at the element level or nodal level. The discretized design variables, denoted $x_i^k, \;\; i = 1, \ldots, m, \;\; k = 1, \ldots, M_i$, represent the density of material i at control point k, where m is the number of candidate materials available in the domain and M_i is the number of control points associated with material i.

In order to ensure existence of solutions and also to avoid numerical artifacts that may result from the discretization of the density fields with possibly unstable finite elements (e.g., checkerboard patterns), a linear kernel filter:

$$F_{jk} = \max\left(0, 1 - \frac{d\left(j,k\right)}{R}\right) \tag{8}$$

is applied to each of the m density fields (Bourdin, 2001; Bruns and Tortorelli, 2001) such that the discrete filtered density field becomes $\hat{x}_i^k = \sum_j w^{jk} x_i^j$ with the weights defined as:

$$w^{jk} = \frac{F_{jk}}{\sum_{l \in Nbhd_k} F_{lk}} \tag{9}$$

In (8) and (9), $d(j,k)$ is the distance between control points x_i^j and x_i^k, R is the radius of the linear filter, and $Nbhd_k = \{x_i^j : d(j,k) \leq R\}$ is the neighborhood of control point x_i^k.

2.4 Statement of the optimization problem

The multi-material compliance minimization problem with arbitrary volume constraints in discretized form and considering up to m candidate materials is stated as:

$$\begin{aligned} \min_{\mathbf{x}_1,\ldots,\mathbf{x}_m} \quad & J = \mathbf{f}^T \mathbf{u}(\hat{\mathbf{x}}_1, \ldots, \hat{\mathbf{x}}_m) \\ \text{s.t.} \quad & g_j = \sum_{i \in \mathcal{G}_j} \sum_{e \in \mathcal{E}_j} \tilde{z}_i^e(\hat{x}_i^k) V^e \leq V_j^{max}, \quad j = 1, \ldots, N_c \\ & 0 \leq x_i^k \leq 1, \quad i = 1, \ldots, m; \;\; k = 1, \ldots, M_i \\ \text{with} \quad & \mathbf{K}(\hat{\mathbf{x}}_1, \ldots, \hat{\mathbf{x}}_m)\, \mathbf{u}(\hat{\mathbf{x}}_1, \ldots, \hat{\mathbf{x}}_m) = \mathbf{f} \end{aligned} \tag{10}$$

where J is structural compliance, g_j are the volume constraints, $\mathcal{G}_j$ is the set of material indices associated with constraint j, $\mathcal{E}_j$ is the set of elements associated with constraint j, $\tilde{z}_i^e$ is the filtered and penalized density of material i in finite element e, V^e is the volume of element e, V_j^{max} is the material volume limit corresponding to constraint j, and N_c is the number of volume constraints.

Note that the volume constraints are defined using filtered and penalized element densities $\tilde{z}_i^e$, but the control points for the design variables x_i^k may be defined as desired, e.g., nodal or element control points. Given x_i^k, the filtered density of material i in element e is defined as:

$$z_i^e\left(\hat{x}_i^k\right) = \frac{1}{n^e} \sum_{k \in \mathcal{K}_e} \hat{x}_i^k \tag{11}$$

where n^e is the number of control points in the set $\mathcal{K}_e$ of control points associated with element e. Note that for nodal control points n_e is equal to the number of nodes on element e and for element control points $n_e = 1$. Then the filtered and penalized element densities are defined as:

$$\tilde{z}_i^e\left(z_i^e\right) = \xi\left(z_i^e\right) \tag{12}$$

where ξ is a penalty function used to drive the material densities toward the 0/1 bounds.

Notice the generality with which the volume constraints may be specified in (10). Each constraint may control the selection of all or a subset of the candidate materials and may be specified for the entire domain or for a sub-region of the domain. Volume constraints were first specified in this way by Zhang et al. (in prep) in the context of ground structures and considering materials with possibly nonlinear behavior.

This work focuses on linear elastic materials. If these materials are also isotropic the optimizer will, in general, select the stiffest of the candidate materials associated with a volume constraint. By including additional information about each material (e.g., mass density or cost), multiple materials may appear in the design (Gao and Zhang, 2011; Wang et al., 2015; Mirzendehdel and Suresh, 2015; Taheri and Suresh, 2016). For example, a scale factor γ_i for each material can be added to the constraint in (10) such that it becomes:

$$g_j = \sum_{i \in G_j} \sum_{e \in E_j} \tilde{z}_i^e(\hat{x}_i^k) \gamma_i V^e \leq M_j^{max} \quad j = 1, \ldots, N_c \tag{13}$$

The scale factor γ_i can be thought of as a mass density or cost of material i and M_j^{max} the mass or monetary limit associated with constraint j. For brevity, the constraint in (13) is interpreted here as a mass constraint and not a cost constraint. It is noted that when $\gamma_i = 1 \;\; \forall i$, the standard volume constraints of (10) are

recovered. By considering mass constraints instead of volume constraints allows e.g., cellular materials, which may be anisotropic, to be considered as candidate materials. In all cases, the optimizer will tend to use all available material such that the volume and/or mass constraints are satisfied in equality.

2.5 Design variable update

The Optimality Criteria (OC) design variable update is widely used for volume constrained compliance minimization problems in two-phase topology optimization because of its simplicity and applicability to problems in which an increase in the quantity associated with the constraint leads strictly to a reduction in the objective. In general, the OC method can only accommodate a single volume constraint, which has led to the use of more complex update schemes, e.g., MMA (Svanberg, 1987), for multi-material topology optimization problems that consider multiple volume constraints (Lund and Stegmann, 2005; Gao and Zhang, 2011; Stegmann and Lund, 2005). However, by studying the primal dual relationship of the linearized version of (10), it has been shown that the design variables associated with each constraint are independent of the other constraints and can be updated via sequential or parallel OC updates for each constraint (Zhang et al., in prep). The key to the validity of this approach is that the Lagrangian is a separable function of the Lagrange multipliers, which in turn requires that the constraints are variable separable.

The OC method is a sequential linear programming technique tailored to the volume constrained compliance minimization problem through intervening variables in the form of $\mathbf{y}_i(\mathbf{x}_i) = \mathbf{x}_i^{-\alpha}$, $\alpha > 0$. With these intervening variables, linearized approximations to (10) are solved using Lagrangian duality at each optimization step. The primal-dual relationship for problems with a single volume constraint has been given, for example, by Christensen and Klarbring (2009) and Groenwold and Etman (2008), and for multiple, volume constraints by Zhang et al. (in prep). The full derivation of the OC design variable update in iteration $t+1$ is repeated here with care to differentiate between unfiltered and filtered design variables, a key to the success of the multi-material design variable update.

The linearized objective at iteration $t+1$ with intervening variables $\mathbf{y}_i(\mathbf{x}_i) = \mathbf{x}_i^{-\alpha}$ is:

$$\tilde{J}\left(\hat{\mathbf{x}}_1, \ldots, \hat{\mathbf{x}}_m\right) = J\left(\hat{\mathbf{x}}_1^t, \ldots, \hat{\mathbf{x}}_m^t\right) + \sum_{i=1}^{m} \left(\left. \frac{\partial J}{\partial \mathbf{y}_i} \right|_{\mathbf{x}_i = \hat{\mathbf{x}}_i^t} \right)^T \left(\mathbf{y}_i\left(\mathbf{x}_i\right) - \mathbf{y}_i\left(\mathbf{x}_i^t\right) \right) \tag{14}$$

Using the chain rule, the derivative of the objective with respect to the intervening variables is evaluated as:

$$\begin{aligned} \left. \frac{\partial J}{\partial y_i^k} \right|_{x_i^k = \hat{x}_i^{k,t}} &= \left(\frac{\partial J}{\partial x_i^k} \frac{\partial x_i^k}{\partial y_i^k} \right) \Bigg|_{x_i^k = \hat{x}_i^{k,t}} \\ &= \left(\frac{\partial J}{\partial x_i^k} \left(-\frac{1}{\alpha} \left(y_i^k \right)^{-\frac{1}{\alpha}-1} \right) \right) \Bigg|_{x_i^k = \hat{x}_i^{k,t}} \\ &= \left. \frac{\partial J}{\partial x_i^k} \right|_{x_i^k = \hat{x}_i^{k,t}} \left(-\frac{\left(\hat{x}_i^{k,t} \right)^{1+\alpha}}{\alpha} \right) \end{aligned} \tag{15}$$

Plugging (15) into (14) and neglecting the constant term in (14), the linearized objective can be written as:

$$\tilde{J}\left(\hat{\mathbf{x}}_1, \ldots, \hat{\mathbf{x}}_m\right) = \sum_{i=1}^{m} \left(-\frac{\left(\hat{\mathbf{x}}_i^t\right)^{1+\alpha}}{\alpha} \left. \frac{\partial J}{\partial \mathbf{x}_i} \right|_{\mathbf{x}_i = \hat{\mathbf{x}}_i^t} \right)^T \left(\mathbf{y}_i(\mathbf{x}_i) - \mathbf{y}_i(\mathbf{x}_i^t) \right) \tag{16}$$

The derivative of the linearized objective in (16) is:

$$\frac{\partial \tilde{J}}{\partial x_i^k} = \left(\frac{\hat{x}_i^{k,t}}{x_i^k} \right)^{\alpha+1} \left. \frac{\partial J}{\partial x_i^k} \right|_{x_i^k = \hat{x}_i^{k,t}} \tag{17}$$

The volume/mass constraints are already linear and can be approximated exactly at iteration $t+1$ by the first two terms in the Taylor series expansion with intervening variables $\mathbf{y}_i(\mathbf{x}_i) = \mathbf{x}_i$:

$$\tilde{g_j} = g_j(\hat{\mathbf{x}}_1^t, \ldots, \hat{\mathbf{x}}_m^t) + \sum_{i \in G_j} \left(\frac{\partial g_j}{\partial \mathbf{x}_i}\bigg|_{\mathbf{x}_i = \hat{\mathbf{x}}_i^t} \right)^T (\mathbf{x}_i - \mathbf{x}_i^t) \tag{18}$$

The derivative of the linearized constraints in (18) are:

$$\frac{\partial \tilde{g_j}}{\partial x_i^k} = \frac{\partial g_j}{\partial x_i^k}\bigg|_{x_i^k = \hat{x}_i^{k,t}} \tag{19}$$

The primal subproblem consists of minimizing the linearized objective (14) subject to the linearized constraints (18):

$$\begin{aligned} \min_{\mathbf{x}_1, \ldots, \mathbf{x}_m} \quad & \tilde{J} = \sum_{i=1}^{m} \left(-\frac{(\hat{\mathbf{x}}_i^t)^{1+\alpha}}{\alpha} \frac{\partial J}{\partial \mathbf{x}_i}\bigg|_{\mathbf{x}_i = \hat{\mathbf{x}}_i^t} \right)^T \left(\mathbf{y}_i(\mathbf{x}_i) - \mathbf{y}_i(\mathbf{x}_i^t) \right) \\ \text{s.t.} \quad & \tilde{g}_j = g_j(\hat{\mathbf{x}}_1^t, \ldots, \hat{\mathbf{x}}_m^t) + \sum_{i \in G_j} \left(\frac{\partial g_j}{\partial \mathbf{x}_i}\bigg|_{\mathbf{x}_i = \hat{\mathbf{x}}_i^t} \right)^T (\mathbf{x}_i - \mathbf{x}_i^t) \leq 0 \\ & 0 \leq x_i^k \leq 1 \end{aligned} \tag{20}$$

The Lagrangian of the primal subproblem is:

$$\begin{aligned} \mathcal{L}(\mathbf{x}_1, \ldots, \mathbf{x}_m, \lambda_1, \ldots, \lambda_{N_c}) &= \sum_{i=1}^{m} \left(-\frac{(\hat{\mathbf{x}}_i^t)^{1+\alpha}}{\alpha} \frac{\partial J}{\partial \mathbf{x}_i}\bigg|_{\mathbf{x}_i = \hat{\mathbf{x}}_i^t} \right)^T \left(\mathbf{y}_i(\mathbf{x}_i) - \mathbf{y}_i(\mathbf{x}_i^t) \right) \\ &\quad + \sum_{j=1}^{N_c} \lambda_j \left(g_j(\hat{\mathbf{x}}_1^t, \ldots, \hat{\mathbf{x}}_m^t) + \sum_{i \in G_j} \left(\frac{\partial g_j}{\partial \mathbf{x}_i}\bigg|_{\mathbf{x}_i = \hat{\mathbf{x}}_i^t} \right)^T (\mathbf{x}_i - \mathbf{x}_i^t) \right) \\ &= \sum_{j=1}^{N_c} \sum_{i \in G_j} \left[\left(-\frac{(\hat{\mathbf{x}}_i^t)^{1+\alpha}}{\alpha} \frac{\partial J}{\partial \mathbf{x}_i}\bigg|_{\mathbf{x}_i = \hat{\mathbf{x}}_i^t} \right)^T \left(\mathbf{y}_i(\mathbf{x}_i) - \mathbf{y}_i(\mathbf{x}_i^t) \right) \right. \\ &\quad \left. + \lambda_j \left(\frac{\partial g_j}{\partial \mathbf{x}_i}\bigg|_{\mathbf{x}_i = \hat{\mathbf{x}}_i^t} \right)^T (\mathbf{x}_i - \mathbf{x}_i^t) \right] + \sum_{j=1}^{N_c} \lambda_j g_j(\hat{\mathbf{x}}_1^t, \ldots, \hat{\mathbf{x}}_m^t) \end{aligned} \tag{21}$$

Using Lagrangian duality, the dual objective can be found using the stationary conditions of the primal subproblem (20). Thus, the dual objective function is:

$$\begin{aligned} \phi(\lambda_1, \ldots, \lambda_{N_c}) &= \min_{0 \leq x_i^k \leq 1} \mathcal{L}(\mathbf{x}_1, \ldots, \mathbf{x}_m, \lambda_1, \ldots, \lambda_{N_c}) \\ &= \sum_{j=1}^{N_c} \left[\min_{0 \leq x_i^k \leq 1} \sum_{i \in G_j} \left(-\frac{(\hat{\mathbf{x}}_i^t)^{1+\alpha}}{\alpha} \frac{\partial J}{\partial \mathbf{x}_i}\bigg|_{\mathbf{x}_i = \hat{\mathbf{x}}_i^t} \right)^T \left(\mathbf{y}_i(\mathbf{x}_i) - \mathbf{y}_i(\mathbf{x}_i^t) \right) \right. \\ &\quad \left. + \lambda_j \left(\frac{\partial g_j}{\partial \mathbf{x}_i}\bigg|_{\mathbf{x}_i = \hat{\mathbf{x}}_i^t} \right)^T (\mathbf{x}_i - \mathbf{x}_i^t) + \lambda_j g_j(\hat{\mathbf{x}}_1^t, \ldots, \hat{\mathbf{x}}_m^t) \right] \end{aligned} \tag{22}$$

Note that the dual objective (22) is separable in such a way that N_c separate minimization problems can be solved and summed:

$$\phi(\lambda_1, \ldots, \lambda_{N_c}) = \sum_{j=1}^{N_c} \phi_j(\lambda_j) \tag{23}$$

The stationary conditions of the separated Lagrangian lead to an explicit formula for the design variable at iteration $t+1$ with the assumption that the box constraints are satisfied:

$$
\begin{aligned}
0 &= \frac{\partial \tilde{J}}{\partial x_i^k} + \lambda_j \frac{\partial \tilde{g}_j}{\partial x_i^k} \\
&= \left(\frac{\hat{x}_i^{k,t}}{x_i^k} \right)^{\alpha+1} \left. \frac{\partial J}{\partial x_i^k} \right|_{x_i^k = \hat{x}_i^{k,t}} + \lambda_j \left. \frac{\partial g}{\partial x_i^k} \right|_{x_i^k = \hat{x}_i^{k,t}} \\
\Rightarrow x_i^k(\lambda_j) &= \hat{x}_i^{k,t} \left(- \frac{\left. \frac{\partial J}{\partial x_i^k} \right|_{x_i^k = \hat{x}_i^{k,t}}}{\lambda_j \left. \frac{\partial g}{\partial x_i^k} \right|_{x_i^k = \hat{x}_i^{k,t}}} \right)^{\frac{1}{\alpha+1}} =: B_i^k(\lambda_j)
\end{aligned}
\tag{24}
$$

Two key ideas become apparent from (24): First, the update of each design variable is dependent only on the Lagrange multiplier of the constraint to which it is associated (Zhang et al., in prep); and second, the numerator in (24) is obtained from (17) and contains only *filtered* densities. Both of these observations are critical to the success of the proposed formulation. Design changes in (24) are controlled and kept within the box constraints using upper and lower bounds $\underline{x}_i^k$ and $\overline{x}_i^k$, respectively:

$$
x_i^k(\lambda_j) = \begin{cases} \underline{x}_i^k & \text{if} \quad B_i^k(\lambda_j) \leq \underline{x}_i^k \\ B_i^k(\lambda_j) & \text{if} \quad \underline{x}_i^k \leq B_i^k(\lambda_j) \leq \overline{x}_i^k \\ \overline{x}_i^k & \text{if} \quad B_i^k(\lambda_j) \geq \overline{x}_i^k \end{cases}
\tag{25}
$$

where the bounds are defined by the move limit, δ:

$$
\underline{x}_i^k = \max \begin{cases} x_i^k - \delta \\ 0 \end{cases} \qquad \overline{x}_i^k = \min \begin{cases} x_i^k + \delta \\ 1 \end{cases}
\tag{26}
$$

In order to find the value of the Lagrange multiplier λ_j in (25), the dual problem is solved using the stationary condition:

$$
\frac{\partial \phi_j}{\partial \lambda_j} = 0 = \frac{\partial \phi_j}{\partial x_i^k} \frac{\partial x_i^k}{\partial \lambda_j} + \frac{\partial \phi_j}{\partial \lambda_j}
\tag{27}
$$

The first term in (27) is zero due to stationary conditions of the Lagrangian and the derivative of the dual objective becomes equal to the linearized constraint of (18) with $\mathbf{x}$ a function of λ_j.

$$
\frac{\partial \phi_j}{\partial \lambda_j} = 0 = g_j \left(\hat{\mathbf{x}}_1^t, \ldots, \hat{\mathbf{x}}_m^t \right) + \sum_{i \in G_j} \left(\left. \frac{\partial g_j}{\partial \mathbf{x}_i} \right|_{\mathbf{x}_i = \hat{\mathbf{x}}_i^t} \right)^T \left(\mathbf{x}_i(\lambda_j) - \mathbf{x}_i^t \right)
\tag{28}
$$

Eq. (28) is monotonic in the interval of interest with $\alpha > 0$, allowing the Lagrange multiplier to be solved for using interval reducing methods, e.g., the bisection method. Note that (28) is independent of the filtered densities at iteration $t+1$, allowing the filter operation to be decoupled from the design variable update (Talischi et al., 2012). This observation has implications on the validity of results obtained when volume/mass constraints control sub-regions of the domain as in Section 5.2.

2.6 Material interpolation

As in two-phase topology optimization, material interpolation functions are used to convert the integer programming problem to a problem of continuous functions for which gradient based optimization techniques can be leveraged. Two commonly used approaches that help push the design variables to the 0/1 bounds are SIMP (Bendsøe, 1989; Zhou and Rozvany, 1991) and RAMP (Rational Approximation of Material Properties, Stolpe and Svanberg (2001)). In the case of up to m candidate materials, penalized element densities for each candidate material are calculated according to (12) with penalty function, $\xi = (z_i^e)^p$ for SIMP or $\xi = z_i^e \,/\, (1 + q\,(1 - z_i^e))$ for RAMP, where $p > 1$ and $q > 0$ are penalty constants that help push the densities

of each material toward zero and one. Note that voids appear when the element densities are zero, i.e., void is not explicitly provided as a candidate material.

For material selection, the penalized densities are coupled with two material interpolation schemes adopted from the DMO techniques (Stegmann and Lund, 2005; Lund and Stegmann, 2005). The DMO material interpolation functions are characterized by a summation of weighted material tensors, i.e, $\eta = \sum_{i=1}^{m} w_i^e \mathbf{C}_i$. In this work, a modified DMO material interpolation is considered:

$$\eta\left(\tilde{\mathbf{z}}^e\right) = \mathbf{C}_{min} + \sum_{i=1}^{m} w_i^e\left(\tilde{\mathbf{z}}^e\right)\left(\mathbf{C}_i - \mathbf{C}_{min}\right) \tag{29}$$

where $w_i^e\left(\tilde{\mathbf{z}}^e\right)$ is the weight of material i in element e, $\mathbf{C}_i$ is the material tensor associated with material i, and $\mathbf{C}_{min}$ helps to avoid singularities in the state equation by adding a small artificial stiffness to $\mathbf{K}$. The goal during the optimization is to find values of the design variables such that a single material weight is active in each element (i.e., $w_i^e = 1$ and $w_{j\neq i}^e = 0, \ \forall e$). The weights are calculated based on the values of the penalized (and filtered) element densities according to the "summation interpolation" or the "product interpolation" by means of an interpolation factor β_i^e:

$$w_i^e\left(\tilde{\mathbf{z}}^e\right) = \tilde{z}_i^e \beta_i^e\left(\tilde{\mathbf{z}}^e\right) \tag{30}$$

where:

$$\beta_i^e\left(\tilde{\mathbf{z}}^e\right) = \begin{cases} 1 & \text{summation interpolation} \\ \prod_{j=1}^{m}\left(1 - \tilde{z}_{j\neq i}^e\right) & \text{product interpolation} \end{cases} \tag{31}$$

In the case of a single solid phase, β_i^e is equal to one for both the summation and product interpolation schemes, and the material interpolation corresponding to SIMP or RAMP for two-phase topology optimization is recovered. It is also noted that regardless of which material interpolation scheme is selected, in this work the total volume V_T^e and density ρ_T^e of material in element e are always calculated as linear functions of the filtered and penalized element densities, i.e., $V_T^e = \sum_{i=1}^{m} \tilde{z}_i^e V^e$ and $\rho_T^e = \sum_{i=1}^{m} \tilde{z}_i^e$. Note that other weighting schemes have been considered; for example Bruyneel (2011) specifies the weights using finite element shape functions.

2.7 Sensitivity analysis

The sensitivity of compliance has been derived as (see e.g., Christensen and Klarbring (2009) for the derivation):

$$\frac{\partial J}{\partial x_i^k} = -\mathbf{u}\left(\mathbf{x}\right)^T \frac{\partial \mathbf{K}}{\partial x_i^k}\mathbf{u}\left(\mathbf{x}\right) \tag{32}$$

Using the chain rule, the derivative of the stiffness matrix with respect to each of the design variables can be computed as:

$$\begin{aligned} \frac{\partial \mathbf{K}}{\partial x_i^k} &= \frac{\partial \mathbf{k}^e}{\partial \tilde{z}_i^e}\frac{\partial \tilde{z}_i^e}{\partial x_i^k} \\ &= \frac{\partial \eta\left(\tilde{\mathbf{z}}^e\right)}{\partial \tilde{z}_i^e}\frac{\tilde{z}_i^e}{x_i^k}\mathbf{k}_o^e \end{aligned} \tag{33}$$

where it has been assumed that the stiffness matrix, $\mathbf{K}$, is assembled from the element stiffness matrices, $\mathbf{k}^e$, which can be expressed as a constant matrix, $\mathbf{k}_o^e$, multiplied by the material interpolation function η for element e:

$$\mathbf{k}^e = \eta\left(\tilde{\mathbf{z}}^e\right)\mathbf{k}_o^e \tag{34}$$

To calculate (33), the derivative of the material interpolation function:

$$\frac{\partial \eta\left(\tilde{\mathbf{z}}^e\right)}{\partial \tilde{z}_i^e} = \begin{cases} \mathbf{C}_i - \mathbf{C}_{min} & \text{summation interpolation} \\ \prod_{j=1}^{m}\left(1-\tilde{z}_{j\neq i}^e\right)\left(\mathbf{C}_i - \mathbf{C}_{min}\right) - \sum_{k=1}^{m}\tilde{z}_{k\neq i}^e \prod_{\substack{l=1 \\ l\neq i}}^{m}\left(1-\tilde{z}_{l\neq k}^e\right)\left(\mathbf{C}_k - \mathbf{C}_{min}\right) & \text{product interpolation} \end{cases} \tag{35}$$

and the derivative of the penalized (and filtered) density for material i in element e:

$$\begin{aligned} \frac{\partial \tilde{z}_i^e}{\partial x_i^k} &= \frac{\partial \xi\left(z_i^e\right)}{\partial z_i^e}\frac{\partial z_i^e}{\partial x_i^k} \\ &= \begin{cases} \frac{p}{n^e}\left(z_i^e\right)^{p-1} & \text{SIMP} \\ \frac{q+1}{n^e\left[1+q\left(1+z_i^e\right)\right]^2} & \text{RAMP} \end{cases} \end{aligned} \tag{36}$$

are needed. Note that in the case of the product interpolation, the material interpolation η and its derivative may be non-positive in regions in which mixing occurs. Although $-\eta$ is non-physical in linear elasticity and leads to problems in the OC design variable update, these mixing regions are small and localized as shown in Section 5.1.1, and neglecting the sensitivities of those design variables does not prevent the product interpolation from yielding reasonable results both qualitatively and quantitatively.

Using the chain rule again, the derivative of the linear volume/mass constraints are:

$$\frac{\partial g_j}{\partial x_i^k} = \frac{\partial g_j}{\partial \tilde{z}_i^e}\frac{\partial \tilde{z}_i^e}{\partial x_i^k} \tag{37}$$

where (36) is used and:

$$\frac{\partial g_j}{\partial \tilde{z}_i^e} = \gamma_i V^e \tag{38}$$

3 Addressing material mixing and total densities greater than unity

The formulation in (10) is characterized by up to m design variables at each control point, each representing the density $x_i^k \in [0,1]$ of one of the candidate materials available at that point. The goal is to find a design in which at most one of the design variables at each control point has value equal to one and the others have zero value. The penalty function ξ serves to push each individual design variable toward zero or one, but does not prevent multiple design variables at a control point from having value simultaneously. To constrain the total density at each control point (e.g., $\sum_{i=1}^{m} x_i^k \leq 1 \ \ \forall k$), as done by Hvejsel and Lund (2011), makes the optimization problem much more complex and is not considered here. Instead, a simple post-processing step is found to be effective.

The summation interpolation simply sums the penalized material densities (at the element level), and thus does not enforce any scheme to ensure that only a single material is present at a given control point. As a result, designs obtained using the summation interpolation often contain large regions of material mixing and total element densities ρ_T^e as large as the number of candidate materials. The product interpolation, however, prevents material mixing through the interpolation factor β_i^e. As is noted by Gao and Zhang (2011), when any one of the weights w_i^k in (30) is exactly equal to one, all other weights must be zero. Thus, in the case that the penalty function is able to push the design variables exactly to their 0/1 bounds, the final design from the product interpolation corresponds to a discrete 0/1 design without any mixing. However, due to the filtering discussed in Section 2.3, intermediate densities appear at material boundaries, leading to mixing at material interfaces and element densities greater than one.

There are multiple ways to post-process depending on desired characteristics of the post-processed design. Two approaches are considered:

1. For each element that contains multiple materials and $\rho_T^e > 1$, assign a density value of one to the material with the greatest contribution to ρ_T^e and a density value of zero to all other materials. This approach will tend to eliminate material mixing, although not strictly enforced.

2. For each element that contains multiple materials and $\rho_T^e > 1$, scale the contribution of each material such that the total element density is equal to one and the relative contributions of the materials remains unchanged. This approach does not eliminate mixing, but removes non-physical situations in which $\rho_T^e > 1$.

A comparison of ρ_T^e before post-processing and $\tilde{\rho}_T^e$ after post-processing for designs obtained using the summation and product interpolation methods are provided in Section 5.1.1 and it is concluded that the product interpolation is not only superior to the summation interpolation, but it provides desirable results that are minimally affected by the described post-processing.

4 Implementation

The multi-material framework presented here is implemented in Sandia National Laboratories' Platform for Topology Optimization (PLATO): an object-oriented, massively parallel framework for optimization-based design (Laboratories, 2016). PLATO's modular framework facilitated the notion of multiple materials to be integrated in a non-invasive manner. This section outlines the core modifications required to extend PLATO to accommodate multiple materials.

4.1 Specifying multi-material input parameters

As in any other density based topology optimization code, PLATO is driven by user specified inputs that define finite element parameters (e.g., domain and finite element mesh, boundary conditions, material specifications, etc.) and topology optimization parameters (e.g., volume limits, penalization scheme, penalty parameters, filter parameters, etc.). PLATO also requires the user to define element blocks, which can consist of the entire mesh or partitions of the mesh. The blocks facilitate specifying things like boundary conditions or non-optimizable regions, but also make it easy to specify the very general volume/mass constraints accommodated by the presented multi-material formulation. Although PLATO can accommodate volume/mass constraints specified in terms of a volume fraction or an absolute volume, this discussion is limited to the former. Each volume/mass constraint is specified by a `vol_frac` keyword followed by the user prescribed value of the volume fraction and two optional lists of materials and blocks that are associated with the constraint. Code Listing 1 shows the syntax used to specify multiple volume constraints as input to PLATO. Of the three entries, only the volume limit is required. If no materials are specified for a given constraint, the constraint controls all optimizable materials. If no blocks are specified for a given constraint, the constraint controls all element blocks.

Code Listing 1: Volume constraint input syntax

```
//volume constraint 1
volf_frac <value> ...                //volume limit, required
   blk <blk_ID> ... blk <blk_ID> ... //associated element blocks, optional
   mat <mat_ID> ... mat <mat_ID>     //associated materials, optional
...
//volume constraint N_c
volf_frac <value> ...                //volume limit, required
   blk <blk_ID> ... blk <blk_ID> ... //associated element blocks, optional
   mat <mat_ID> ... mat <mat_ID>     //associated materials, optional
```

In specifying the list of volume/mass constraints, it is important to ensure that each design variable is associated with only a single constraint. For example, two volume/mass constraints specifying only the value of the volume/mass limit (i.e., no materials or element blocks are specified) is invalid because both constraints would attempt to control all of the design variables simultaneously. It is also important to ensure that if multiple volume/mass constraints control a single element block, that the values of the volume/mass

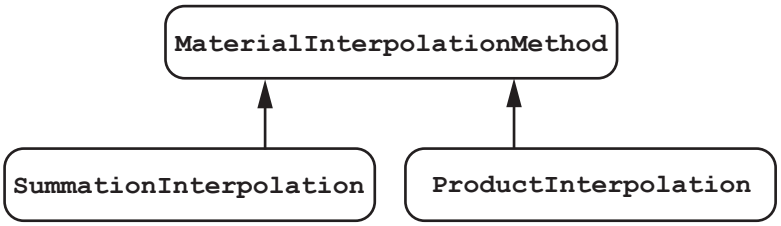

Figure 2: `MaterialInterpolationMethod` class hierarchy

limits controlling that element block sum to less than one. Based on the specified volume/mass constraints, PLATO computes the initial guess for the multi-material topology optimization such that distribution of density to each material in a given constraint is uniform, i.e., no material is favored at initialization.

4.2 Material interpolation abstract class

Code Listing 2 shows the blueprint for the abstract class, `MaterialInterpolationMethod`, that performs the material interpolation in PLATO. The class specifies two pure virtual functions `computeMultiMaterialFactor`() and `computeMultiMaterialSensitivity`(), which are implemented by subclasses for the two DMO material interpolation schemes: `SummationInterpolation` and `ProductInterpolation`. The class hierarchy is provided in Fig. 2. `computeMultiMaterialFactor`() returns the material interpolation factor β_i^e in (31), which is used with the existing `Penalty_Model` class to interpolate the material tensors according to (29). `computeMultiMaterialSensitivity`() takes pre-assembled element stiffness matrices $\mathbf{k}_o^e$ as input and performs the sensitivity calculation of (33), (35), and (36), returning the derivatives to be used directly in (32) for the sensitivity of compliance.

Code Listing 2: MaterialIterpolationMethod class blueprint

```
class MaterialInterplationMethod {
public:
   //constructor, etc.
   // ...
   virtual double computeMultiMaterialFactor(
      const size_t material_index_,
      const size_t block_index_,
      const std::vector<std::vector<double> >& elem_control_vectors_) const = 0;
   virtual void computeMultiMaterialSensitivity(
      const size_t material_index_;
      const size_t block_index_,
      const size_t ele,ent_index_,
      const std::vector<std::vector<double> >& elem_control_vectors,
      double** element_sensitivity_) const = 0;
};
```

4.3 Optimality Criteria implementation

Since each design variable is dependent only on the Lagrange multiplier of the constraint it is associated with, the design variables can be updated one constraint at a time, in an arbitrary order. PLATO parses the inputs described above in such a way that the program knows which design variables are associated with which constraint. As such, a loop is implemented over the design variable update scheme such that it is called N_c times, each time only passing the design variables and associated sensitivities corresponding to constraint j. Algorithm 1 provides the pseudo-code for the Optimality Criteria design variable update considering multiple volume/mass constraints.

Algorithm 1 Optimality Criteria algorithm considering multiple materials

for $j = 1$ to N_c **do**
  Initialize bisection interval lower bound, λ_j^l
  Initialize bisection interval upper bound, λ_j^u
  while $\left(\lambda_j^u - \lambda_j^l\right) / \left(\lambda_j^u + \lambda_j^l\right) >$ tolerance **do**
    update Lagrange multiplier λ_j of constraint j (bisection)
    update design variables $x_i^k\left(\lambda_j\right)$ associated with constraint j (Eq. 25)
    if derivative of j^{th} term of the dual problem > 0 (Eq. 28) **then**
      reset interval lower bound, $\lambda_j^l = \lambda_j$
    else
      reset interval upper bound, $\lambda_j^u = \lambda_j$
    end if
  end while
end for

Table 1: Optimization parameters

SIMP penalty parameter, p	3
filter radius, R	2
OC move limit, δ	0.2
OC linearization exponent, α	2
convergence tolerance	0.008

5 Numerical examples

Two numerical examples are presented to demonstrate the key features, capabilities, and limitations of the presented formulation for multi-material topology optimization. Both examples are based on a 2D MATLAB implementation with control points defined at the elements.

All candidate materials are fully dense and without associated costs ($\gamma_i = 1 \ \ \forall i$) unless stated otherwise. Since all candidate materials are also linear elastic and isotropic, the material tensor $\mathbf{C}_i$ for material i can be specified by two scalar parameters: modulus of elasticity E_i and Poisson's ratio ν_i. An ersatz stiffness $E_{min} = 1 \times 10^{-9}$ is used to define $\mathbf{C}_{min}$ in all examples. All of the examples use the SIMP penalty function and the optimization parameters provided in Table 1 are used for all designs. The specified convergence tolerance defines the acceptable magnitude of change in design variables (infinity norm) used as a stopping criterion for the optimization algorithm. It is also noted that the formulation performs best when the initial guess does not favor any one candidate material. Thus, in all examples, the initial guess is specified such that all of the elements have an equal initial density of each candidate material and the volume/mass constraint is satisfied in equality.

The plots provided for all of the 2D results are surface plots with the x- and y-axes in the plane of the design and the z-axis representing the filtered and penalized density of each material. Intermediate densities below 0.3 are not plotted.

5.1 2D MBB beam

The MBB beam is used to provide some discussion on and/or demonstration of the following items:

1. a comparison between the summation and product material interpolation methods, highlighting the effect of post-processing;

2. the ability of the formulation to accommodate many materials through an example specifying up to five separate volume constraints for each of up to five candidate materials in the entire domain;

3. the ability of the formulation to obtain multi-material designs with specification of a single global mass constraint that controls multiple candidate materials in the entire domain by considering candidate

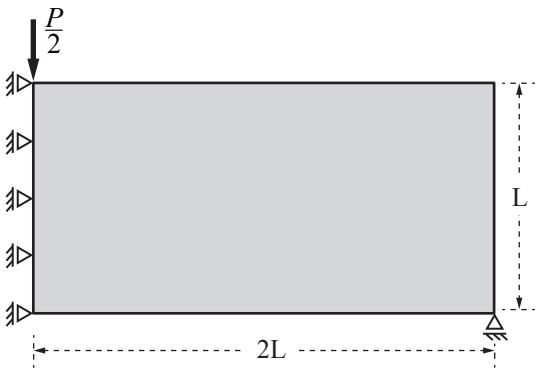

Figure 3: MBB beam domain and boundary conditions (symmetry assumed along the left edge)

Table 2: MBB beam candidate material properties

		Modulus of Elasticity, E_i	Poisson's Ratio, ν_i
	material 1	1	0.3
	material 2	0.8	0.3
	material 3	0.5	0.3
	material 4	0.4	0.3
	material 5	0.2	0.3

materials with varying stiffness-to-mass ratios.

The domain and boundary conditions for the half-MBB beam are provided in Fig. 3 and the parameters considered are $L = 60$ and $P = 1$. The domain is discretized into a 120×60 orthogonal finite element mesh composed of four-node quadrilateral elements. Symmetry along the left edge of the domain is assumed and results are shown with symmetry imposed. Material properties for five candidate materials considered in the MBB beam results to follow are provided in Table 2.

5.1.1 2D MBB beam: Comparison of summation and product material interpolation methods

In this section, the MBB beam is designed considering a volume constraint for each of three candidate materials: materials 1, 3, and 5 of Table 2. The volume limits V_j^{max}, $j = 1, \ldots, 3$ are specified such that each of the candidate materials can occupy no more than one-sixth of the design domain (see the volume fraction limits for the 3-material design in Table 3). As a result, the final design is expected to occupy 1/2 of the domain.

Although the summation and product material interpolation methods lead to designs with similar compliance, the convergence history shown in Fig. 4 indicates that the two methods follow different paths toward an optimal solution, leading to different designs. In Fig. 5(a) and (b) the total element densities

Table 3: Multi-material MBB beam design: specified volume fractions for 2, 3, 4, and 5-material designs

		2-material design	3-material design	4-material design	5-material design
	material 1	1/4	1/6	1/8	1/10
	material 2	–	–	1/8	1/10
	material 3	1/4	1/6	–	1/10
	material 4	–	–	1/8	1/10
	material 5	–	1/6	1/8	1/10

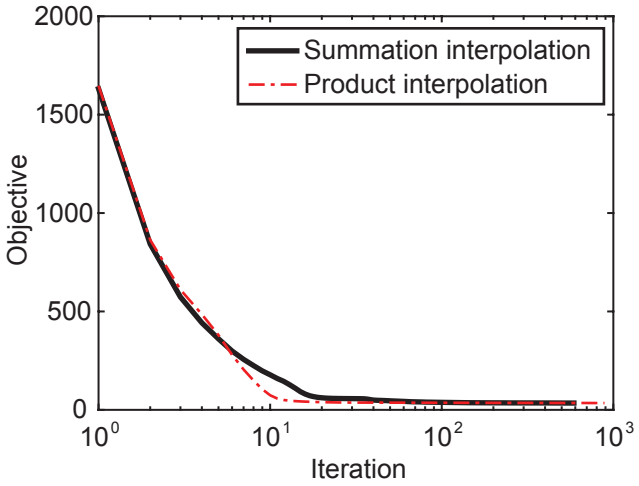

Figure 4: Convergence plot for the summation and product material interpolation schemes for the MBB beam design considering candidate materials 1, 3, and 5 each constrained to occupy no more than 1/6 of the domain.

ρ_T^e at convergence are provided considering the summation and product material interpolation methods, respectively. The converged result based on the summation interpolation (Fig. 5(a)) contains large regions of material mixing in the portions of the beam where the largest strains are expected. Since there is no means to penalize material mixing, ρ_T^e reaches a maximum value of 3 in these regions, indicating that all design variables are at their upper bounds. Material mixing is also observed in the converged design based on the product interpolation (Fig. 5(b)); however, it is limited to regions where distinct materials come together and the magnitudes of ρ_T^e tend to be less than the number of material phases at the junction. In fact, the material mixing in the case of the product rule is due to intermediate densities along the material boundaries that result from filtering.

Both of the post-processing approaches discussed in Section 3 are applied to the two designs. The post-processed total element densities $\tilde{\rho}_T^e$ are shown in Fig. 5(c) and (d) for the summation and product interpolation methods, respectively. The compliance J and the total material volume fraction are summarized in Table 4 for the converged design and after post-processing. Because of the large regions of material mixing in which $\rho_T^e = m$, post-processing on the result of the summation interpolation leads to a significant reduction in total volume relative to the converged result and increases in the objective function that are especially large with the post-processing approach 2. In contrast, the reduction in total volume and the change in the objective tends to be small when using the product interpolation.

In general, the product material interpolation method leads to more robust results, and thus, will be used exclusively in the remaining examples. Although post-processing approach 2 leads to an increased objective relative to convergence in this example, it seems reasonable from a physical standpoint to allow mixing at the intersection of materials. As such, all multi-material designs provided in the following sections are plotted after post-processing with approach 2. However, the quantitative results provided are based on the converged results since the change in compliance and volume is negligible (and the considered post-processing will never lead to a violation of the volume constraint).

5.1.2 2D MBB beam: Separate volume constraints for an arbitrary number of material phases

To demonstrate that the presented formulation is effective for an arbitrary number of material phases, the MBB beam is designed considering a volume constraint for each of two, three, four, and five of the candidate materials in Table 2. The formulation can accommodate more than five materials, but the specified volume fraction of each material becomes too small to yield desirable results. V_j^{max} is specified according to the volume fractions provided in Table 3. The post-processed (approach 2) designs considering the product material interpolation are provided in Fig. 6. Note that the design in Fig. 6(b) corresponds to that of Fig. 5(d) and similar plots of post-processed total element densities in which the maximum $\tilde{\rho}_T^e = 1$ could

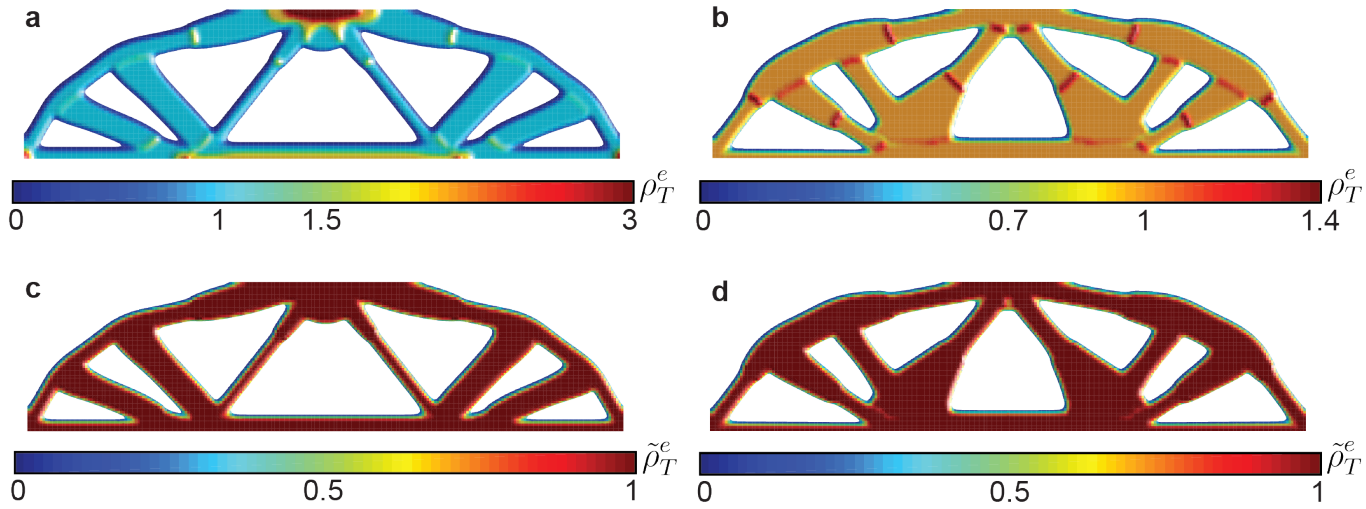

Figure 5: 3-material MBB beam design: total element densities ρ_T^e for converged results based on the (a) summation material interpolation and (b) product material interpolation; total element densities $\tilde{\rho}_T^e$ for post-processed results based on the (c) summation material interpolation and (d) product material interpolation. Note: $\tilde{\rho}_T^e$ is the same for both post-processing approaches

Table 4: 3-material MBB beam design: comparison of compliance and total material volume fraction before and after post-processing for both the summation and product material interpolation methods

	summation interpolation		product interpolation	
	compliance, J	total material volume fraction	compliance, J	total material volume fraction
at convergence	34.54	0.5	34.59	0.5
post-processed (approach 1)	39.39	0.437	33.58	0.494
post-processed (approach 2)	111.79	0.437	36.02	0.494

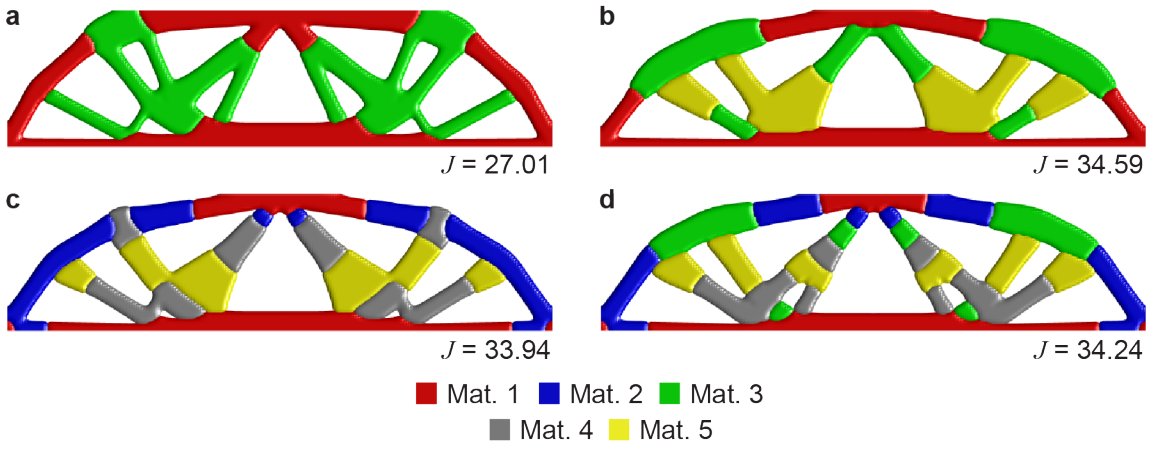

Figure 6: Multi-material MBB beam designs with each material indicated by color: (a) 2 materials; (b) 3 materials; (c) 4 materials; (d) 5 materials. All results consider the product material interpolation and the plots are after applying post-processing approach 2

be obtained for the other three designs (i.e., $\tilde{\rho}_T^e \leq 1 \ \ \forall e$ in Fig. 6). The depressions at the intersections of material phases shown in Fig. 6 indicate material mixing and not that the total element density is less than one.

The results in Fig. 6 also demonstrate that the presented formulation leads to results that make intuitive sense from a mechanics perspective. In all cases, the stiffest material is distributed to the regions of the beam where strains are expected to be highest, while the more compliant materials are distributed toward the neutral axis where strains are expected to be low. In fact, in the four and five material designs (Fig. 6(c) and (d)), distinct horizontal "layers" of materials are observed: the most compliant materials are located toward the middle while the most stiff are toward the top and bottom surfaces. It is noted that the examples in this section apply equal volume limits to each candidate material, but the formulation is equally as effective for arbitrary volume limits on each of the candidate materials.

5.1.3 2D MBB beam: Single mass constraint for 2-material design

For linear elastic, isotropic materials with a single volume constraint controlling all of the materials, the optimizer will always select the stiffest material for the minimum compliance problem. In the previous two sub-sections, multi-material designs were obtained by imposing separate volume constraints on each of the candidate materials, allowing all of the available materials to emerge and be used to their limits. In this sub-section, scale factors ($\gamma_i \neq 1, \ \ i = 1, \ldots, m$) are applied to a single mass constraint and it is shown that multi-material designs can be obtained even when all materials are controlled by a single constraint. By varying the stiffness-to-mass ratios of the candidate materials, the optimizer may select a more compliant material in favor of a less dense material. Although not explicitly considered here, cellular materials may have varying stiffness-to-mass ratios and could be considered as candidate materials in the present formulation.

The MBB beam is designed this time considering candidate materials 1 and 2 from Table 2. For all cases the stiffness-to-mass ratio of material 1 is held constant ($E_1/\gamma_1 = 1$), while that of material 2 is varied. Although arbitrary, the mass limit used here is defined such that $M^{max} = \min(\gamma_i) V^{max}$, where V^{max} is the actual volume limit. Defining the mass limit in this way leads to designs with total volume equal to V^{max} when the entire structure consists of the least dense material and total volume less than V^{max} when the entire structure consists of the material with highest mass density or when multiple materials arise in the design. In all cases, the total mass obeys the mass limit M^{max}, which tends to be satisfied in equality.

Designs considering four different stiffness-to-mass ratios of material 2 are provided in Fig. 7 and the corresponding volume, mass, and compliance for each are provided in Table 5. V^{max} is specified such that no more than 3/5 of the domain can be filled with material. When $E_1/\gamma_1 = E_2/\gamma_2$ a single-material design consisting of only the stiffest material is obtained (Fig. 7(a)). As the stiffness-to-mass ratio of the more compliant material 2 is increased by reducing γ_2, an increasing volume of material 2 is obtained in the final

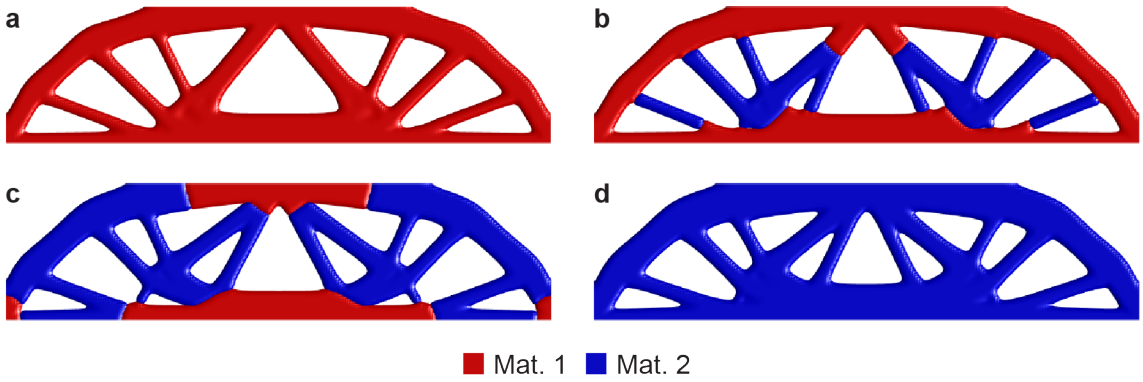

Figure 7: 2-material MBB beam design with $E_1/\gamma_1 = 1$ and varying stiffness-to-mass ratio for material 2: (a) $E_2/\gamma_2 = 1$; (b) $E_2/\gamma_2 = 1.01$; (c) $E_2/\gamma_2 = 1.03$; (d) $E_2/\gamma_2 = 3$. All results consider the product material interpolation and the plots are after applying post-processing approach 2

Table 5: Volume fractions v_i of each material, mass $\gamma_i v_i$ of each material, and compliance J for each of the MBB beam designs considering candidate materials 1 and 2 and a single global mass constraint with $E_2/\gamma_2 = 1$ and varying stiffness to mass-ratio for material 2. All numerical results consider the product material interpolation and are obtained at convergence before applying any post-processing

Figure	E_2/γ_2	V^{max}	M^{max}	v_1	v_2	$\sum_{i=1}^{m} v_i$	$\gamma_1 v_1$	$\gamma_2 v_2$	$\sum_{i=1}^{m} \gamma_i v_i$	J
7(a)	1	0.6	0.480	0.480	0	0.480	0.480	0	0.480	22.101
7(b)	1.01	0.6	0.475	0.354	0.153	0.507	0.354	0.121	0.475	22.344
7(c)	1.03	0.6	0.466	0.159	0.396	0.555	0.159	0.308	0.466	22.088
7(d)	3	0.6	0.160	0	0.600	0.600	0	0.160	0.160	22.262

design. Fig. 7(b) is based on $E_2/\gamma_2 = 1.01$ and Fig. 7(c) is based on $E_2/\gamma_2 = 1.03$. If the stiffness-to-mass ratio is large enough, it becomes more economical to use only the more compliant material (Fig. 7(d)) by allowing for a larger volume of material while still satisfying the mass constraint. Notice that the compliance for each of the designs in Fig. 7 is almost identical, while the volume increases and mass decreases as E_2/γ_2 increases.

5.2 2D mid-rise building bracing design: Controlling distribution of facade openings through volume constraints on subregions

The previous examples demonstrated the effectiveness of the proposed formulation to accommodate multiple volume/mass constraints that can control a subset of the candidate materials (Section 5.1.2) or all candidate materials simultaneously (Section 5.1.3). In both of the previous cases, the volume/mass constraints control the material distribution in the entire domain. In this section, a mid-rise building of width 90 and height 240 is designed considering a single material ($E_1 = 1$, $\nu_1 = 0.3$) and volume constraints are defined to control sub-regions of the domain. Five cases are considered: one, six, twelve, twenty-four, and ninety-six subregions (see Fig. 8), each with a volume constraint limiting the material in a sub-region from occupying more than 1/2 of the sub-region volume. In each case the boundary conditions of Fig. 8(a) are applied: fixed support at the base and eleven equal point loads of magnitude 0.1 applied along the height of the building on both sides to mimic a simplified wind loading. The same finite element discretization is also used in all cases: 90 $\times$ 240 four-node quadrilateral finite elements.

The resulting designs are provided in Fig. 9, where it is shown that for a single sub-region (Fig. 9(a)) the material tends to concentrate in the bottom half of the structure and as the number of specified sub-regions increases, the material becomes more uniformly distributed throughout the domain. In the case of building bracing design, specifying volume constraints on sub-regions of the domain enables the designer to obtain

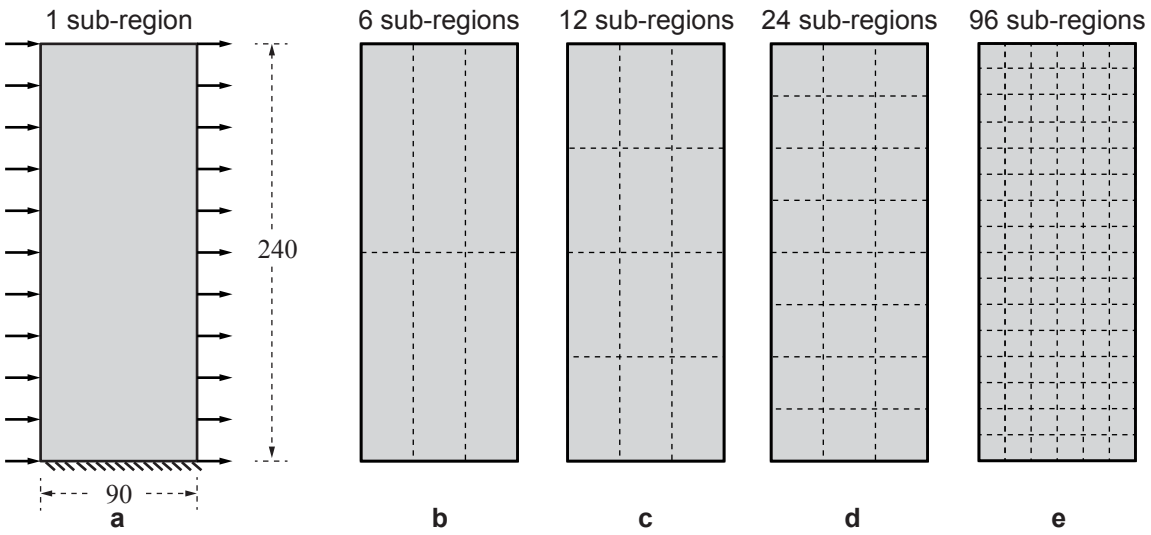

Figure 8: Mid-rise building bracing design: (a) domain and boundary conditions with one sub-region; (b) six sub-regions; (c) twelve sub-regions; (d) twenty-four sub-regions; and (e) ninety-six sub-regions.

solutions with more evenly distributed material throughout the domain, achieving designs with more uniform lighting emitted into the interior space. Note that the total volume fraction of material is 1/2 in each of the final designs in Fig. 9, but the compliance increases as the number of sub-regions increases since more constraints are imposed on the problem.

One additional note is that the sub-regions are not visible in the final designs in Fig. 9, i.e, the material smoothly transitions from one sub-region to the next. This feature is a direct result of the observation that the stationary condition of the dual sub-problem in (28) is independent of filtered densities and as such the filter operation is decoupled from the design variable update (Talischi et al., 2012).

6 Conclusions

A simple and robust formulation for multi-material topology optimization in the continuum setting is presented that can accommodate an arbitrary number of materials and arbitrarily specified volume/mass constraints. Specifically, by taking advantage of the separable dual objective in the linearized subproblems used for the design variable update, the standard Optimality Criteria method can be applied for each volume/-mass constraint, one at a time, in parallel or in series. The formulation allows for multiple volume/mass constraints that can control all or a subset of the candidate materials in the entire domain or a subset of the domain. Results with up to five solid material phases are presented and shown to make sense from a mechanics perspective, but the formulation itself places no limits on the number of materials that can be considered. It is also shown that by specifying volume constraints on subregions of the domain, a designer can obtain increased control over the material distribution at the expense of increased compliance for a more highly constrained problem. Although the number of design variables increases linearly with the number of candidate materials, the variable separability of constraints defined in accordance with a DMO material interpolation allows for an efficient design variable update scheme. Additional constraints to ensure that pointwise densities do not exceed one are not considered and it is shown that a simple post-processing step is sufficient to achieve physical designs that are almost identical to the converged design. (Might be nice to tie conclusion back to the discussion on additive manufacturing in the introduction...Would be really nice to print some of these designs)

7 Acknowledgments

Need to write this section...

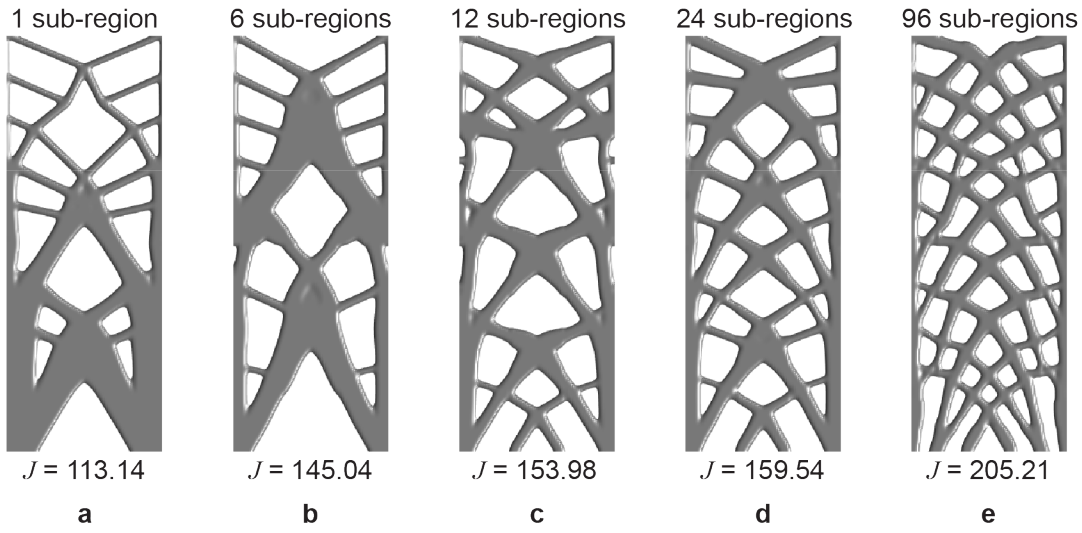

Figure 9: Mid-rise building bracing design with (a) one sub-region; (b) six sub-regions; (c) twelve sub-regions; (d) twenty-four sub-regions; and (e) ninety-six sub-regions

Nomenclature

α	linearization exponent
$\bar{t}$	prescribed traction
$\bar{u}$	prescribed displacement
β_i^e	material interpolation factor for material i in element e
χ	indicator function
δ	Optimality Criteria move limit
$\delta\mathbf{u}$	test functions
$\delta\Omega$	boundary of Ω
η	material interpolation function
γ_i	scale factor representing mass density of material i
Γ_t	partition of $\delta\Omega$ where tractions are prescribed
Γ_u	partition of $\delta\Omega$ where displacements are prescribed
λ_j	Lagrange multiplier of constraint j
$\mathbf{C}(\mathbf{X})$	spatially varying material tensor
$\mathbf{C}_i$	material tensor associated with material i
$\mathbf{C}_{min}$	material tensor contributing small artificial stiffness
$\mathbf{f}$	vector of applied nodal forces
$\mathbf{K}$	stiffness matrix
$\mathbf{k}^e$	element stiffness matrix

$\mathbf{k}_o^e$ constant portion of element stiffness matrix

$\mathbf{u}$ displacement field (trial functions)

$\mathbf{X} \in \mathbb{R}^{n_{sd}}$ material point

$\mathbf{y}_i$ intervening variable

$\mathcal{A}$ choice function

$\mathcal{E}_j$ set of elements associated with constraint j

$\mathcal{G}_j$ set of material indices associated with constraint j

$\mathcal{K}_e$ set of control points associated with element e

$\mathcal{L}$ Lagrangian function

ν_i Poisson's ratio of material i

Ω set of material points in design domain

ω set of material points defining optimal shape

ϕ dual objective

$\rho_i(\mathbf{X})$ continuous density field for material i

$\rho_T(\mathbf{X})$ total density of material at material point $\mathbf{X}$

ρ_T^e total density of material in element e

$\tilde{\rho}_T^e$ total density of material in element e after post-processing

$\tilde{g}_j$ linearized constraint j

$\tilde{J}$ linearized objective

$\tilde{z}_i^e$ filtered and penalized density of material i in element e

$\underline{x}_i^k$, $\overline{x}_i^k$ lower and upper bounds on x_i^k during the design variable update

ξ penalty function

B_R ball of radius R

$d(j,k)$ distance between control points x_i^j and x_i^k

E_i modulus of elasticity of material i

E_{min} ersatz stiffness

F filter

g_j j^{th} volume/mass constraint

J objective function

m number of candidate materials available in the domain

M_i number of control points associated with material i

M_j^{max} mass limit associated with constraint j

$m_{\mathbf{X}}$ number of candidate materials at material point $\mathbf{X}$

n number of finite element in the design domain

N_c number of volume/mass constraints

n_e number of control points in set $\mathcal{K}_e$

N_i shape function for degree of freedom i

n_{sd} spatial dimension

$Nbhd_j$ neighborhood of control point j

p penalty parameter for SIMP

q penalty parameter for RAMP

R filter radius

$S(\mathbf{X})$ set of material tensors for the candidate materials at material point $\mathbf{X}$

t traction

U set of kinematically admissible displacement fields

U_o set of test functions

V^e volume of element e

V_j^{max} volume or mass limit corresponding to constraint j

v_j^{max} volume fraction limit of constraint j

v_T total volume fraction of all materials

V_T^e total volume of material in element e

v_T^{max} total material volume fraction limit

w_i^e weight of material i in element e

w_i^{jk} linear filter weight between control points j and k

x_i^k density of material i at control point k

z_i^e filtered density of material i in element e

References

M. P. Bendsøe. Optimal shape design as a material distribution problem. *Structural Optimization*, 1(4): 193–202, 1989.

B. Bourdin. Filters in topology optimization. *International Journal for Numerical Methods in Engineering*, 50(9):2143–2158, 2001.

T. E. Bruns and D. A. Tortorelli. Topology optimization of non-linear elastic structures and compliant mechanisms. *Computer Methods in Applied Mechanics and Engineering*, 190(26):3443–3459, 2001.

M. Bruyneel. Sfpa new parameterization based on shape functions for optimal material selection: application to conventional composite plies. *Structural and Multidisciplinary Optimization*, 43(1):17–27, 2011.

P. W. Christensen and A. Klarbring. *An Introduction to Structural Optimization*. Springer, Linköping, 2009.

E. T. Filipov, J. Chun, G. H. Paulino, and J. Song. Polygonal multiresolution topology optimization (polymtop) for structural dynamics. *Structural and Multidisciplinary Optimization*, 53(4):673–694, 2016.

T. Gao and W. Zhang. A mass constraint formulation for structural topology optimization with multiphase materials. *International Journal for Numerical Methods in Engineering*, 88(8):774–796, 2011.

A. T. Gaynor, N. A. Meisel, C. B. Williams, and J. K. Guest. Multiple-material topology optimization of compliant mechanisms created via polyjet three-dimensional printing. *Journal of Manufacturing Science and Engineering*, 136(6):061015, 2014.

L. V. Gibiansky and O. Sigmund. Multiphase composites with extremal bulk modulus. *Journal of the Mechanics and Physics of Solids*, 48(3):461 – 498, 2000. ISSN 0022-5096. doi: http://dx.doi.org/10.1016/S0022-5096(99)00043-5. URL `http://www.sciencedirect.com/science/article/pii/S0022509699000435`.

A. A. Groenwold and L. Etman. On the equivalence of optimality criterion and sequential approximate optimization methods in the classical topology layout problem. *International journal for numerical methods in engineering*, 73(3):297–316, 2008.

X. Guo, W. Zhang, and W. Zhong. Stress-related topology optimization of continuum structures involving multi-phase materials. *Computer Methods in Applied Mechanics and Engineering*, 268:632–655, 2014.

X. Huang and Y. Xie. Bi-directional evolutionary topology optimization of continuum structures with one or multiple materials. *Computational Mechanics*, 43(3):393–401, 2009.

C. F. Hvejsel and E. Lund. Material interpolation schemes for unified topology and multi-material optimization. *Structural and Multidisciplinary Optimization*, 43(6):811–825, 2011.

C. F. Hvejsel, E. Lund, and M. Stolpe. Optimization strategies for discrete multi-material stiffness optimization. *Structural and Multidisciplinary Optimization*, 44(2):149–163, 2011.

S. N. Laboratories. Plato. http://www.sandia.gov/plato3d/index.html, 2016.

E. Lund and J. Stegmann. On structural optimization of composite shell structures using a discrete constitutive parametrization. *Wind Energy*, 8(1):109–124, 2005.

A. M. Mirzendehdel and K. Suresh. A pareto-optimal approach to multimaterial topology optimization. *Journal of Mechanical Design*, 137(10):101701, 2015.

T. H. Nguyen, G. H. Paulino, J. Song, and C. H. Le. A computational paradigm for multiresolution topology optimization (mtop). *Structural and Multidisciplinary Optimization*, 41(4):525–539, 2010.

T. H. Nguyen, G. H. Paulino, J. Song, and C. H. Le. Improving multiresolution topology optimization via multiple discretizations. *International Journal for Numerical Methods in Engineering*, 92(6):507–530, 2012.

J. Park and A. Sutradhar. A multi-resolution method for 3d multi-material topology optimization. *Computer Methods in Applied Mechanics and Engineering*, 285:571–586, 2015.

C. Schumacher, B. Bickel, J. Rys, S. Marschner, C. Daraio, and M. Gross. Microstructures to control elasticity in 3d printing. *ACM Trans. Graph.*, 34(4):136:1–136:13, July 2015. ISSN 0730-0301. doi: 10.1145/2766926. URL `http://doi.acm.org/10.1145/2766926`.

O. Sigmund. Design of multiphysics actuators using topology optimization–part ii: Two-material structures. *Computer methods in applied mechanics and engineering*, 190(49):6605–6627, 2001.

O. Sigmund and S. Torquato. Design of materials with extreme thermal expansion using a three-phase topology optimization method. *Journal of the Mechanics and Physics of Solids*, 45(6):1037 – 1067, 1997. ISSN 0022-5096. doi: http://dx.doi.org/10.1016/S0022-5096(96)00114-7. URL `http://www.sciencedirect.com/science/article/pii/S0022509696001147`.

J. Stegmann and E. Lund. Discrete material optimization of general composite shell structures. *International Journal for Numerical Methods in Engineering*, 62(14):2009–2027, 2005.

M. Stolpe and K. Svanberg. An alternative interpolation scheme for minimum compliance optimization. *Struct Multidisc Optim*, 22(2):116–124, 2001.

Stratasys. Polyjet technology. `http://www.stratasys.com/3d-printers/technologies/polyjet-technology`, 2016. Accessed: 2016-12-06.

K. Svanberg. The method of moving asymptotes-a new method for structural optimization. *International Journal of Numerical Methods in Engineering*, 24:359–373, 1987.

A. H. Taheri and K. Suresh. An isogeometric approach to topology optimization of multi-material and functionally graded structures. *International Journal for Numerical Methods in Engineering*, 2016.

C. Talischi, G. H. Paulino, A. Pereira, and I. F. Menezes. Polytop: a matlab implementation of a general topology optimization framework using unstructured polygonal finite element meshes. *Structural and Multidisciplinary Optimization*, 45(3):329–357, 2012.

R. Tavakoli and S. M. Mohseni. Alternating active-phase algorithm for multimaterial topology optimization problems: a 115-line matlab implementation. *Structural and Multidisciplinary Optimization*, 49(4):621–642, 2014.

S. Vatanabe, G. Paulino, and E. Silva. Design of functionally graded piezocomposites using topology optimization and homogenization–toward effective energy harvesting materials. *Computer Methods in Applied Mechanics and Engineering*, 266:205–218, 2013.

S. L. Vatanabe, G. H. Paulino, and E. C. N. Silva. Influence of pattern gradation on the design of piezocomposite energy harvesting devices using topology optimization. *Composites Part B: Engineering*, 43(6): 2646–2654, 2012.

S. L. Vatanabe, G. H. Paulino, and E. C. Silva. Maximizing phononic band gaps in piezocomposite materials by means of topology optimization. *The Journal of the Acoustical Society of America*, 136(2):494–501, 2014.

M. Wallin, N. Ivarsson, and M. Ristinmaa. Large strain phase-field-based multi-material topology optimization. *International Journal for Numerical Methods in Engineering*, 104(9):887–904, 2015.

M. Y. Wang and X. Wang. color level sets: a multi-phase method for structural topology optimization with multiple materials. *Computer Methods in Applied Mechanics and Engineering*, 193(6):469–496, 2004.

M. Y. Wang and S. Zhou. Synthesis of shape and topology of multi-material structures with a phase-field method. *Journal of Computer-Aided Materials Design*, 11(2-3):117–138, 2004.

M. Y. Wang, S. Chen, X. Wang, and Y. Mei. Design of multimaterial compliant mechanisms using level-set methods. *Journal of Mechanical Design*, 127(5):941–956, 2005.

Y. Wang, Z. Luo, Z. Kang, and N. Zhang. A multi-material level set-based topology and shape optimization method. *Computer Methods in Applied Mechanics and Engineering*, 283:1570–1586, 2015.

L. Yin and G. Ananthasuresh. Topology optimization of compliant mechanisms with multiple materials using a peak function material interpolation scheme. *Structural and Multidisciplinary Optimization*, 23 (1):49–62, 2001.

T. Zegard and G. H. Paulino. Bridging topology optimization and additive manufacturing. *Structural and Multidisciplinary Optimization*, 53(1):175–192, 2016.

X. Zhang, A. S. Ramos Jr., and G. H. Paulino. Multi-material nonlinear topology optimization using the ground structure method. *Journal of Structural and Multidisciplinary Optimization*, in prep.

M. Zhou and G. Rozvany. The coc algorithm, part ii: topological, geometrical and generalized shape optimization. *Computer Methods in Applied Mechanics and Engineering*, 89(1-3):309–336, 1991.

S. Zhou and M. Y. Wang. Multimaterial structural topology optimization with a generalized cahn–hilliard model of multiphase transition. *Structural and Multidisciplinary Optimization*, 33(2):89–111, 2007.